NANO LETTERS

pubs.acs.org/NanoLett Letter

Manipulating Redox Kinetics of Sulfur Species Using Mott−Schottky Electrocatalysts for Advanced Lithium−Sulfur Batteries

Yuanjian Li,[⊥] Wenyu Wang,[⊥] Bao Zhang,[⊥] Lin Fu, Mintao Wan, Guocheng Li, Zhao Cai, Shuibin Tu, Xiangrui Duan, Zhi Wei Seh, Jianjun Jiang, and Yongming Sun*

Cite This: https://doi.org/10.1021/acs.nanolett.1c02161 Read Online

ACCESS | Metrics & More | Article Recommendations | Supporting Information

ABSTRACT: Lithium−sulfur (Li−S) batteries suffer from sluggish sulfur redox reactions under high-sulfur-loading and lean-electrolyte conditions. Herein, a typical Co@NC heterostructure composed of Co nanoparticles and a semiconductive N-doped carbon matrix is designed as a model Mott−Schottky catalyst to exert the electrocatalytic effect on sulfur electrochemistry. Theoretical and experimental results reveal the redistribution of charge and a built-in electric field at the Co@NC heterointerface, which are critical to lowering the energy barrier of polysulfide reduction and Li_2S oxidation in the discharge and charge process, respectively. With Co@NC Mott−Schottky catalysts, the Li−S batteries display an ultrahigh capacity retention of 92.1% and a system-level gravimetric energy density of 307.8 Wh kg^{-1} under high S loading (10.73 mg cm^{-2}) and lean electrolyte (E/S = 5.9 μL mg_{sulfur}^{-1}) conditions. The proposed Mott−Schottky heterostructure not only deepens the understanding of the electrocatalytic effect in Li−S chemistry but also inspires a rational catalyst design for advanced high-energy-density batteries.

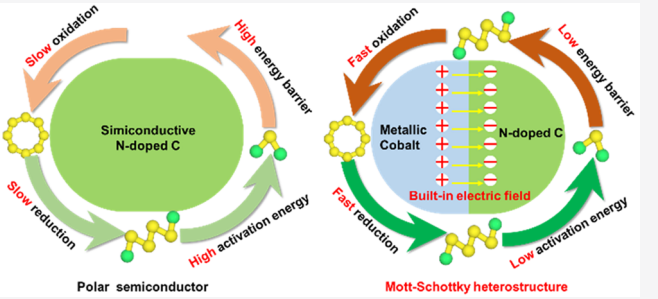

KEYWORDS: *Mott−Schottky heterostructure, lithium−sulfur batteries, catalytic polysulfide conversion, lean electrolyte conditions*

Lithium-sulfur (Li−S) batteries have drawn tremendous academic and industrial interests due to the natural abundance of sulfur feedstock and ultrahigh intrinsic energy density (≈2600 Wh kg^{-1}).[1,2] Such high specific energy derives from sulfur-related redox reactions that involve the reduction of solid sulfur molecules (S_8) to form solid lithium sulfide (Li_2S) with a series of dissolvable lithium polysulfides (LiPSs) intermediates on discharge and a reversible oxidation process on charge.[3,4] However, this multiphase sulfur conversion chemistry faces some intrinsic challenges, including undesirable "shuttling" behavior of polysulfides and sluggish sulfur redox reactions.[5,6] Introducing electrocatalyst into sulfur cathode has shown great potential in expediting polysulfides reduction in charge process[7,8] and/or Li_2S oxidation in discharge process,[9,10] thus efficiently suppressing polysulfide diffusion out of the cathode. Benefiting from this electrocatalysis effect, the lifespan and capacity of Li−S batteries have been updated to an acceptable level (>1000 cycles and >1300 mAh g^{-1}) over the past few years.[11,12] These achievements, however, are usually obtained under a low sulfur loading (<4 mg cm^{-2}) and excess electrolyte (E/S > 15 μL mg_{sulfur}^{-1}), leading to low cell-level energy density (often <200 Wh kg^{-1}).[13,14] Moreover, the exploration and discovery of catalysts mainly rely on trial and error, and the underlying catalytic mechanism in Li−S conversion chemistry still lacks deep mechanistic understanding.[15,16]

In Li−S electrochemistry, the kinetics of conversion reactions among sulfur species are strongly determined by surface adsorption and deposition as well as charge/mass transfer at the three-phase interface among catalysts, sulfur species, and electrolytes.[17] These heterogeneous reactions intrinsically depend on the catalyst's surface electronic states. For most inorganic materials (such as N-doped C,[18] CoP,[15,19] TiO_2,[20] MoS_2,[21] and C_3N_4[22,23]), although they can immobilize polysulfides through a chemisorption mechanism, their semiconducting nature jeopardizes the electron transport to the surface-bonded polysulfide and the subsequent redox reactions of sulfur species (Figure 1a).[24] To this end, coupling these semiconductors with metallic phases as Mott−Schottky heterojunctions could be a proof-of-concept method to boost the catalytic activity by optimizing interfacial electronic interactions (Figure 1b). From basic semiconductor physics, the different energy structures between metal and semiconductor can drive the flow of electrons across the interface until the heterojunctions reach the thermodynamic equilibrium

Received: June 2, 2021
Revised: July 16, 2021

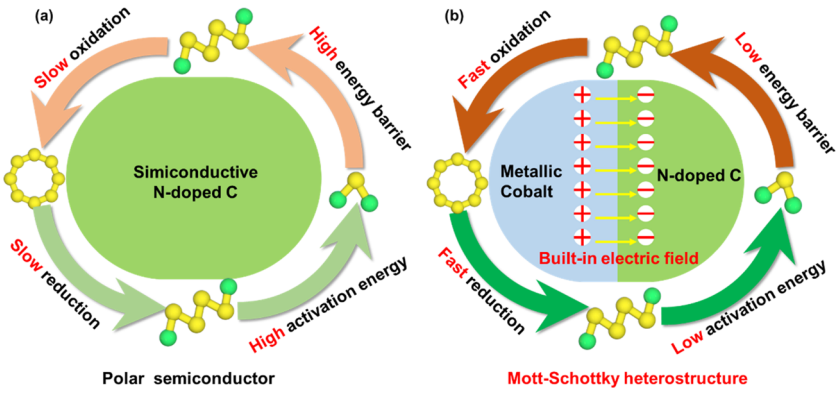

Figure 1. Schematic for Li−S batteries with different cathode hosts: (a) routine polar semiconductor and (b) Mott−Schottky heterostructures.

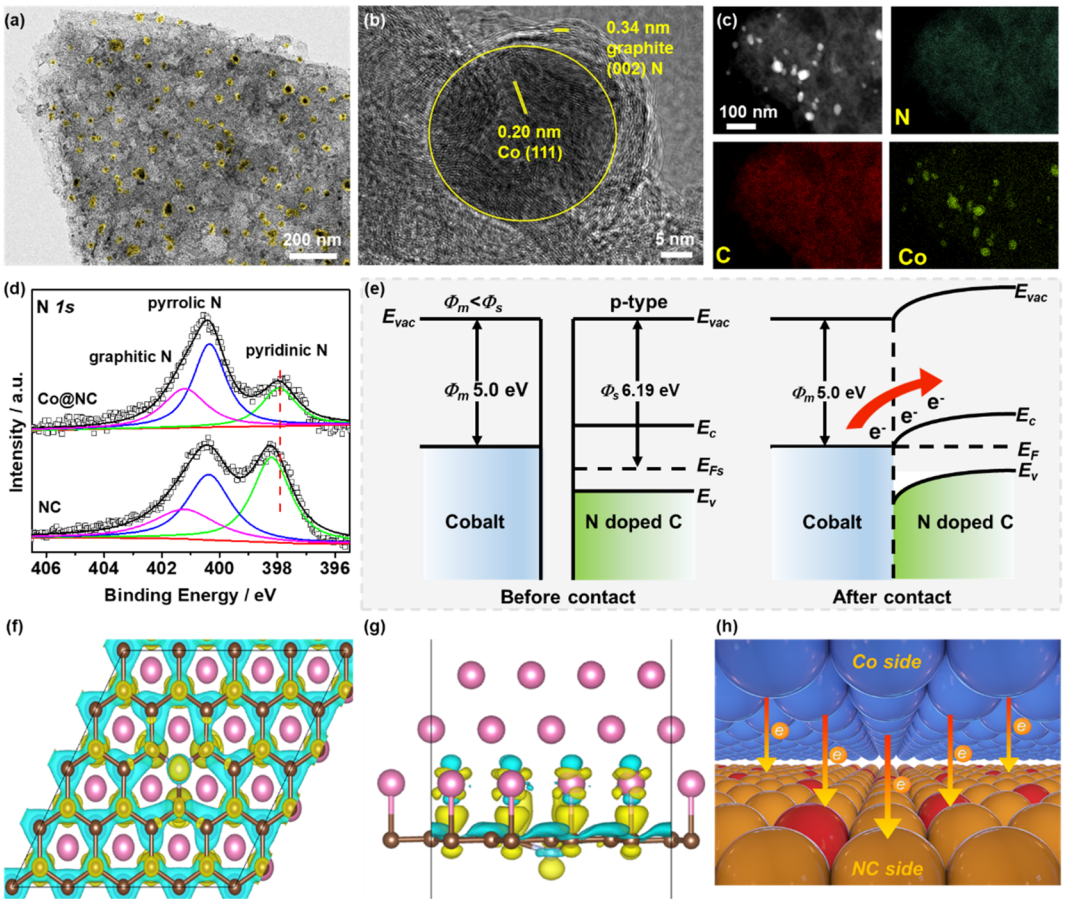

Figure 2. (a) TEM, (b) HRTEM, (c) HAADF images, and the corresponding EDX mapping results of the Co@NC heterostructure. (d) N 1s XPS spectra of NC and Co@NC. (e) Schematic illustration of the Mott−Schottky type contact of the Co@NC before and after contacting. (f, g) Differential charge density redistributions in the Co@NC heterostructure. The yellow and blue isosurfaces represent charge accumulation and depletion in the space, respectively, and the isosurface level is 0.002 au. (h) Schematic diagram for the charge transfer between Co and NC.

state.[25,26] This manipulation of electron transfer in Mott−Schottky heterojunction can induce charge separation and an internal electric field at the interface, which not only propels the charge transfer and ion diffusion in lithium-ion batteries[27] but also modulates the energy barriers of photo/electrocatalytic reactions.[25,28] Despite these advances, catalytic understanding of Mott−Schottky heterostructure for Li−S conversion chemistry is rarely explored, yet critical to electrocatalysts design for sulfur-based battery technology.

To investigate the Mott−Schottky effect on conversion chemistry in Li−S batteries, herein, we put forward a paradigmatic Co@NC heterostructure consisting of Co nanoparticles encapsulated in a porous N-doped carbon matrix as a sulfur cathode host. Both spectroscopy techniques and computational simulations demonstrate that the metallic character of cobalt can derive spontaneous rearrangement of the NC substrate's energy band, which facilitates charge transfer and induces a strong built-in electric field at the interface of Co@NC heterostructure. These interfacial merits of Co@NC Mott−Schottky electrocatalysts are beneficial to strengthening adsorption and conversion of polysulfides as well as lowering the energy barriers of sulfur reduction in the

https://doi.org/10.1021/acs.nanolett.1c02161
Nano Lett. XXXX, XXX, XXX−XXX

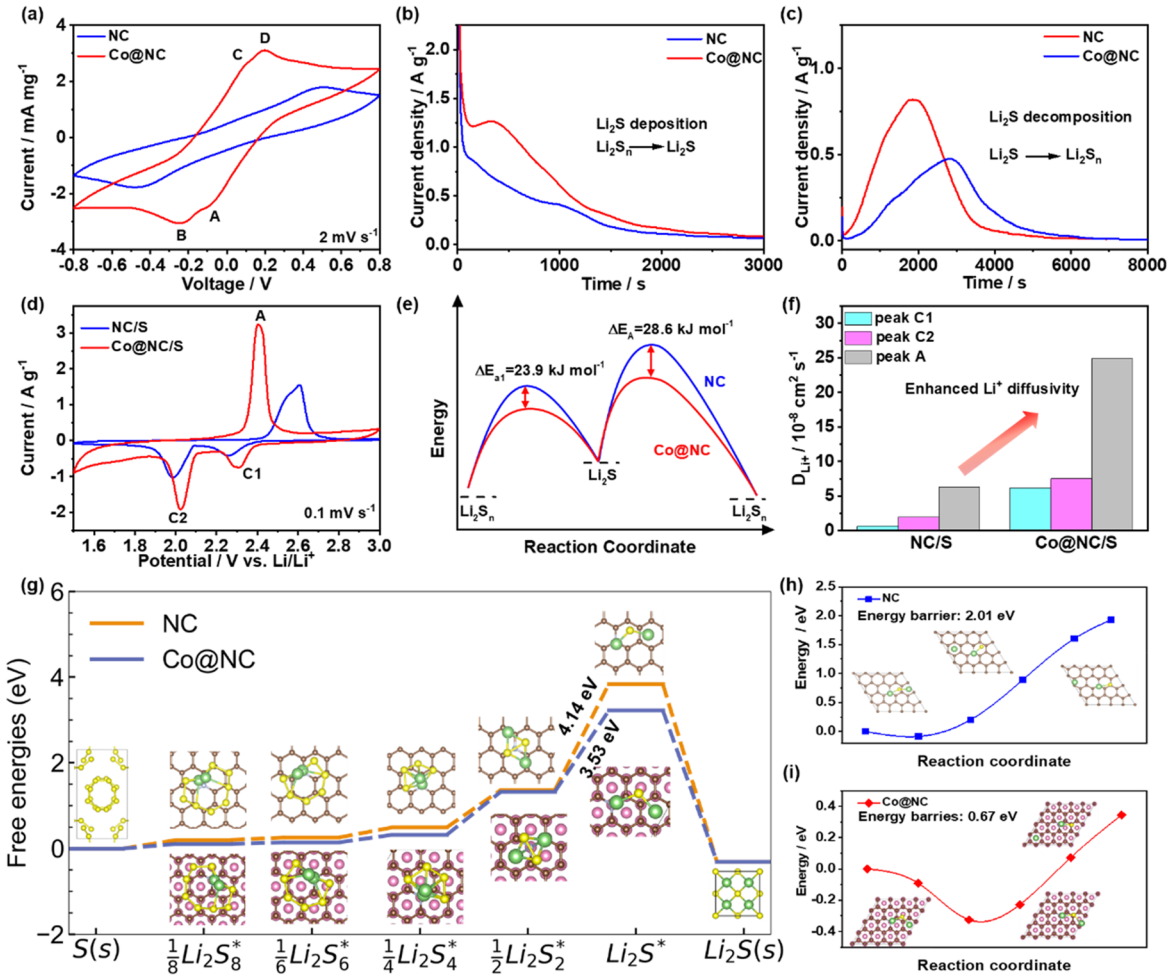

Figure 3. (a) CV profiles of Li_2S_6 symmetrical cells with NC and Co@NC electrodes. (b) Potentiostatic discharge profiles with a Li_2S_6 solution from the open-circuit voltage to 2 V. (c) Potentiostatic charge profile at 2.40 V to evaluate dissolution kinetics of Li_2S. (d) CV profiles of Li−S batteries with NC/S and Co@NC/S cathodes. (e) The activation energies (E_a) of the formation and dissolution of Li_2S. (f) Li^+ diffusion coefficient calculated from the Randles−Sevcik equation. Free-energy evolution for (g) S reduction and (h, i) decomposition of a Li_2S cluster on NC and Co@NC supports, where the optimized adsorption configurations of polysulfide species and the initial, transition, and final structures of Li_2S are presented in the inset. The black, yellow, green, pink, and dark blue balls represent C, S, Li, N, and Co atoms, respectively.

discharge process and Li_2S oxidation in the charge process. Consequently, the thus-derived Co@NC electrocatalyst renders Li−S batteries with remarkable cyclicity and gravimetric energy density under harsh test conditions, such as large current density of 4 C, ultrahigh sulfur loading of 10.73 mg cm^{-2}, low electrolyte/sulfur ratio of 5.9 μL mg^{-1}. The present work depicts the intriguing potential of rationally designed Mott−Schottky electrocatalysts for advanced Li−S batteries.

The Co@NC catalyst was synthesized through a facile metal−organic framework-templated method (Figure S1) and possessed a two-dimensional (2D) leaf-like morphology with a length of ∼5 μm, a width of ∼3 μm, and a thickness of ∼200 nm (Figure S2). Transmission electron microscopy (TEM) observation image (Figure 2a) discloses a porous and rough surface of the 2D product with embedded cobalt nanoparticles. The average diameter of the embedded Co nanoparticles is ∼10 nm (Figure S3). Figure 2b shows the high-resolution TEM of Co@NC heterostructure, where the lattice fringe of 0.20 nm accounts for the (111) plane of metallic cobalt. The encapsulated graphitic carbon shells have an average thickness of 4 nm and a lattice fringe of 0.34 nm, corresponding to its (002) plane.[27] X-ray diffraction and Raman analysis (Figures S4 and S5) further confirm the coexistence of Co and graphitic carbon in the Co@NC composites. The energy-dispersive X-ray spectroscopy (EDX) investigations (Figure 2c) imply the uniform distribution of Co nanoparticles inside the porous nitrogen−carbon framework. Such a porous structure has a large surface area (410.7 m^2 g^{-1}) and an average mesopore size (∼4.5 nm) (Figure S6), which is beneficial for loading ample sulfur. The weight percentage of Co nanoparticles is determined to be 11.6% by thermogravimetric analysis (TGA) (Figure S7).

The chemical environments of Co@NC heterostructure were examined by X-ray photoelectron spectroscopy (XPS). As depicted in Figure S8b, the high-resolution Co $2p_{3/2}$ spectrum can be divided into two sub-bands at 778.5 and 780.3 eV, corresponding to metallic Co and Co−N species, respectively.[29] The N 1s spectrum in Figure 2d is resolved into pyridinic N (397.9 eV), pyrrolic N (400.4 eV), and graphitic N (401.1 eV).[30] The successful incorporation of N into the carbon matrix can also be confirmed by the C 1s spectrum (Figure S8d), in which a peak at 285.3 eV of characteristic C−N bonding is fitted. For comparison, pure Co metal and pure

https://doi.org/10.1021/acs.nanolett.1c02161
Nano Lett. XXXX, XXX, XXX−XXX

N-doped graphitic carbon (NC) counterparts (Figures S9 and S10) were also tested under identical conditions. We note that there is no characteristic Co−N peak for the pure Co sample (Figure S8b), which supports the interaction of Co and N species and accordingly positively charged Co species in Co@NC junction. Notably, the pyridinic N and C−N peaks of the NC sample are positively shifted to 398.1 and 285.6 eV in comparison with those of the Co@NC (Figure 2d and Figure S8c).[31] Namely, NC species in the Co@NC compound have a negative charge after metallic Co decoration. The above XPS results strongly reveal the electronic interactions between Co and NC, causing the injection of electrons from Co to NC at their coupling interfaces.

The surface electron transfer in Co@NC heterostructure is strongly affected by the work functions of the Co and NC, according to the band theory of solids.[26] According to ultraviolet photoelectron spectroscopy (UPS) results (Figure S11), the work function of Co@NC and NC is calculated to be 5.88 and 6.19 eV, respectively. Since the N-doped C has a p-type semiconductor structure,[26] when a semiconducting NC is directly contacted with metallic Co with a smaller work function (5.00 eV), the electrons from Co will spontaneously move to NC until the same Fermi levels are reached on both sides. This self-driven charge density redistribution on the heterointerfaces is also known as the Mott−Schottky effect in solid-state physics.[28]

The behavior of electron transfer between Co and NC was further theoretically elucidated by Bader charge analysis. The simulated Co@NC heterostructure model in Figure 2f,g explicitly illustrates the strong interfacial polarization between Co and NC and accordingly injection of electrons from surface Co atom to adjacent N atoms in NC, thus resulting in a built-in electric field pointing toward NC, which agree well with the experimental results (Figure 2h). In Li−S chemistry, this structural merit contributes to the chemical LiPSs-binding ability of Co@NC heterostructur since the negatively charged NC side can improve adsorption of Li^+ while the positively charged Co side is prone to adsorb polysulfide anions.[32] This conclusion is confirmed by a visual Li_2S_6 adsorption experiment (Figure S12) and additional XPS analyses of Co@NC/Li_2S_6 composites (Figure S13). This strong interaction between Co@NC and polysulfides is important for inhibiting the polysulfides shuttling and accelerating their subsequent conversion in Li−S batteries.

To determine the effectiveness of Mott−Schottky heterostructure in boosting polysulfide-involving reactions, cyclic voltammetry (CV) of symmetrical cells based on Co@NC and NC catalysts were analyzed in Li_2S_6 electrolyte. As exhibited in Figure 3a, four distinct redox peaks can be detected from the Co@NC cell, while the NC cell only exhibits an inconspicuous pair of redox peaks. The profile discrepancy of CV results strongly validates the kinetics advantage of Co@NC for polysulfide redox conversion over NC. The electrochemical impedance spectroscopy (EIS) results (Figure S15) further reveal the high catalytic capability of Co@NC that can reduce the charge transfer resistance (R_{ct}) at the Co@NC/polysulfides interface. Subsequently, the kinetic evaluation of liquid−solid conversion from polysulfide to Li_2S was monitored by Li_2S precipitation in a potentiostatic discharge experiment.[33] As observed from the I−t curves in Figure 3b, the Li_2S nucleation peak possesses a higher current of 1.26 A g^{-1} after 310 s on the Co@NC electrode over that of NC electrode (0.41 A g^{-1} after 1010 s), indicating that the Co@NC electrocatalyst significantly improved the kinetics of Li_2S nucleation and deposition. The solid−liquid conversion from Li_2S to polysulfide was performed likewise by a potentiostatic charge method (Figure 3c).[33] Similarly, the Co@NC electrode exhibits shorter nucleation times (1850 s) and higher charging current responses (0.82A g^{-1}) compared to the NC counterpart (0.48 A g^{-1} after 2760 s), pointing to propelled Li_2S dissolution kinetics on Co@NC catalysts. Primarily, the results signify that the Mott−Schottky effect on Co@NC heterojunction can catalyze all phase polysulfide-involving processes.

The superior electrocatalytic activity and hierarchical porous structure render the Co@NC Mott−Schottky electrocatalyst to be an auspicious cathode sulfur host. Through a melt-infusion method, Co@NC/sulfur composites with 74.5 wt % sulfur were fabricated (Figure S15−S17). The resulting Co@NC/S cathode presents typical Li−S redox reactions,[34] where the CV profile (Figure 3d) shows two cathodic peaks appear at 2.308 (peak C1) and 2.025 V (peak C2) and an anodic peak (peak A) at 2.404 V. With respect to the NC@S cathode, it exhibits the lower CV current and larger polarization between peak C1 and A as compared with the Co@NC/S cathode, suggesting a more rapid sulfur conversion kinetics in working Li−S batteries owing to the Mott−Schottky effect of Co@NC catalyst. To quantify the catalytic activity of the Co@NC catalyst, the Tafel plots were calculated according to corresponding CV curves. As shown in Figure S20, the Co@NC/S cathodes are characterized by lower Tafel slopes for both Li_2S_n-to-Li_2S (69.2 mV dec^{-1}) and Li_2S-to-Li_2S_n (63.5 mV dec^{-1}) steps than those of the NC/S cathodes (106.0 and 103.1 mV dec^{-1}, respectively), further demonstrating the significant kinetic promotion of sulfur species in both charging and discharging processes upon Mott−Schottky effect.[35] Activation energy (E_a) is also an important fundamental parameter for evaluating Li−S conversion chemistry.[16,36] Accordingly, we fitted the charge-transfer resistance measured at various temperatures into the Arrhenius equation, and the E_a was derived to be 46.3 and 67.9 kJ mol^{-1} for Co@NC/S NC/S cathode, respectively (Figure S21).[7] Pertaining to the reduction of Li_2S_n into Li_2S, the rate-limiting step in the discharge process, the E_a difference between the Co@NC/S and NC/S cathodes is 23.9 kJ mol^{-1} based on the Tafel analysis (see details in the Experiment section) (Figure 3e).[36] Likewise, the calculated E_a of Co@NC/S cathode for the Li_2S oxidation process is 28.6 kJ mol^{-1} smaller than that of NC/S cathode. These dramatically reduced E_a values indicate that the reversible reactions between polysulfides and Li_2S are thermodynamically more favorable on the Co@NC Mott−Schottky junction.

The fact that sulfur redox reactions in Li−S batteries are always accompanied by Li-ion transfer encourages us to study the diffusivity of Li^+ at the Co@NC interface. Through CV testing at 0.1 to 0.5 mV s^{-1}, the lithium-ion diffusion coefficient (D_{Li+}) can be calculated to be 6.17×10^{-8}, 7.55×10^{-8}, and 2.49×10^{-7} cm^2 s^{-1} for the Co@NC/S cathode at peaks C1, C2, and A, respectively, which are an order of magnitude larger than those of NC/S cathode ($6.37\times 10^{-9} \sim 6.28\times 10^{-8}$ cm^2 s^{-1}), as shown in Figure 3f and S22. The enhanced Li^+ diffusion properties on the Co@NC/S surface may be attributed to three advantages of the Co@NC host: (1) porous architecture that shortens ion transport path; (2) in-built electric field in the Co@NC heterointerface that offers Li^+ transfer pathways; (3) the barrier energy for Li^+ transfer on

https://doi.org/10.1021/acs.nanolett.1c02161
Nano Lett. XXXX, XXX, XXX−XXX

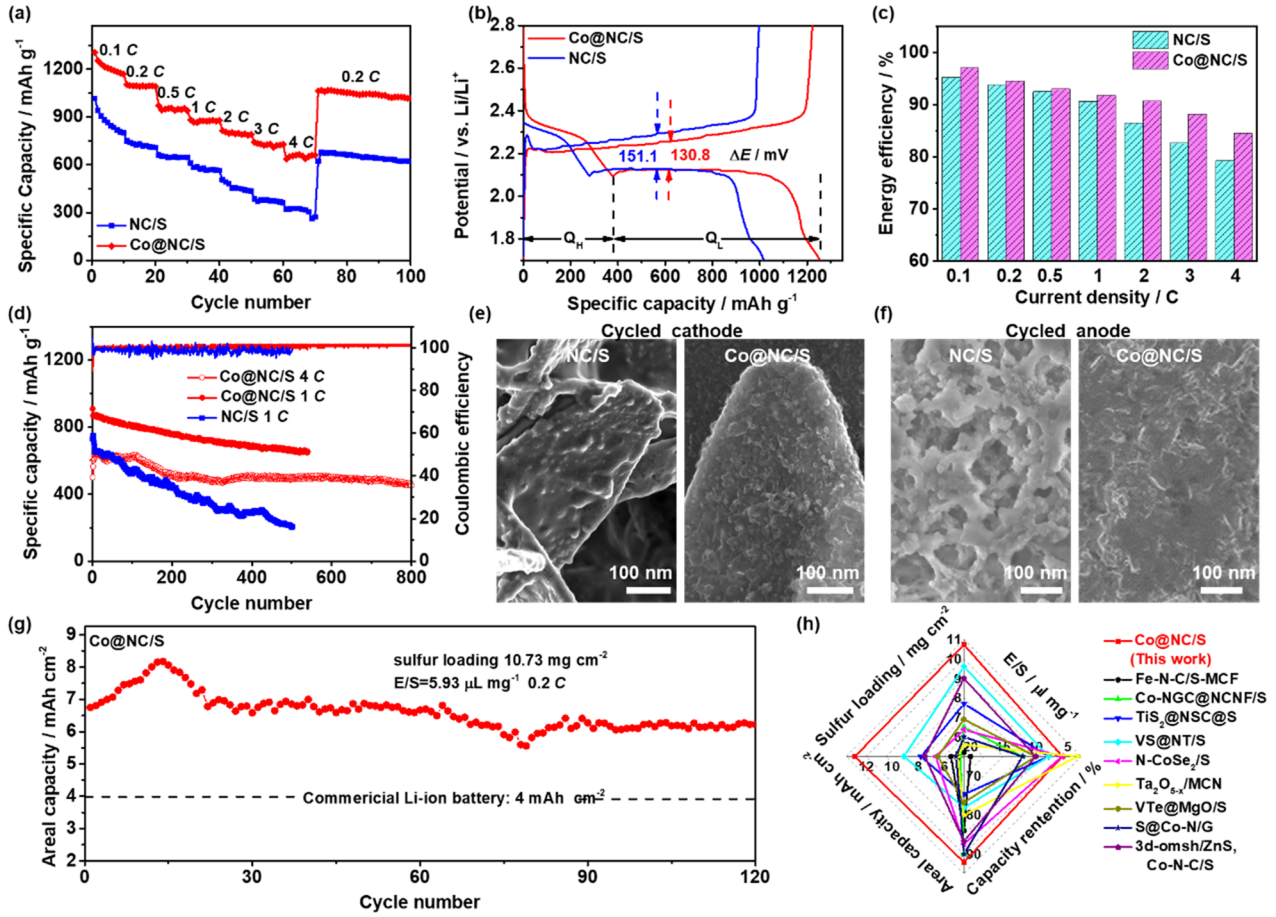

Figure 4. (a) Rate capabilities of NC/S and Co@NC/S cathodes. (b) Charge/discharge curves of different electrodes at 0.1 *C*. (c) Energy efficiency of different cathodes. (d) Long-term cycling performance of different cathodes at 1 and 4 *C*. SEM images of the (e) sulfur cathode and the (f) Li anode after 100 cycles at 1 *C*. (g) Cycling performance of the Co@NC/S cathode with a high sulfur mass loading of 10.73 mg cm^{-2} at 0.2 *C*. (h) Electrochemical performance comparison between our Co@NC/S cathode and previously reported sulfur cathodes. The related data are collected from Table S2.

the Co (111) surface is theoretically estimated to be almost 10 times smaller than that on NC surface.[37]

We also carried out density functional theory (DFT) calculations to simulate the oxidation and reduction reactions of sulfur electrochemistry on both NC and Co@NC substrates. The results in Figure 3g exhibit that the transformation of S_8 to Li_2S during discharge involves four intermediate LiPSs, namely, Li_2S_8, Li_2S_6, Li_2S_4, and Li_2S_2. Due to its largest positive Gibbs free (ΔG), the Li_2S_2-to-Li_2S step is determined to be the rate-limiting step among all the steps, consistent with previous reports.[38] The ΔG for the formation of Li_2S on Co@NC is 3.53 eV, much smaller than that on NC (4.14 eV), clearly demonstrating that the reduction of S_8 is much easier on the Co@NC surface. Figure 3h and i decipher the energy profiles of Li_2S decomposition during charge, which starts from an intact Li_2S molecule and ends with a LiS cluster and a single Li-ion and electron ($Li_2S \rightarrow LiS + Li^+ + e^-$).[9,38] The energy barriers for Li_2S decomposition on NC and Co@NC surfaces are calculated to be 0.67 and 2.01 eV, respectively. The lower energy barrier evidence the catalytic effects of Co@NC heterostructure for boosting Li_2S phase transformation. These theoretical simulations, together with the above electrochemical analysis, evidently explain the Mott−Schottky effect on the Co@NC can simultaneously catalyze the S reduction and Li_2S oxidation, which is crucial to expedite the electrochemical properties of Li−S energy storage systems.

After validating the superiority of the Co@NC Mott−Schottky electrocatalyst, the electrochemical properties of Li−S cells using Co@NC/S cathodes were then evaluated. The rate capability of Co@NC/S cathode with a sulfur mass loading of 1.5 mg cm^{-2} is presented in Figure 4a. The discharge specific capacities are as high as 1303, 1103, 971, 882, 815, 741, and 634 mAh g^{-1} at 0.1, 0.2, 0.5, 1, 2, 3, and 4 *C*, respectively, suggesting excellent rate capability of the Co@NC/S electrode. When skipping back the current rate to 0.2 *C*, the discharge capacity can be recovered to 1064 mAh g^{-1}, indicative of good stability and structural robustness. All these discharge capacities are much higher than those of NC/S (4 *C*, 320 mAh g^{-1}) cathode. Figure 4b and S23 compare charge/discharge curves at different current rates, from which one can observe higher capacities of both high- and low-voltage plateau (Q_H and Q_L) as well as the larger ratio of Q_L/Q_H for the Co@NC/S cathode than those of NC/S cathode especially at faster rates, revealing that polysulfides species are effectively captured and converted by the Co@NC host. During the charge process, a lower discharge voltage and the disappeared voltage jump for Co@NC/S cathode in comparison with NC/S cathode confirms the superior catalytic activity of the Co@NC heterostructure toward the kinetic oxidation process of Li_2S.[38]

https://doi.org/10.1021/acs.nanolett.1c02161
Nano Lett. XXXX, XXX, XXX−XXX

Furthermore, it is worth noting that the voltage differences (ΔE) between the charge and the second discharge plateaus of the Co@NC/S electrode are significantly lower than those of the NC/S electrode at all current rates (Figure S24c). This decrease of cell polarization also contributes to the increase in energy efficiency (Figure 4c), which further confirms that the Co@NC Mott−Schottky electrocatalyst effectively propels the kinetics of round-trip sulfur redox reactions ($S_8 \leftrightarrow S_6^{2-} \leftrightarrow S_4^{2-} \leftrightarrow Li_2S_2 \leftrightarrow Li_2S$) in a working cell.[23]

The Co@NC Mott−Schottky electrocatalyst also improved the prolonged cycling stability of sulfur cathodes. As shown in Figure 4d, the Co@NC/S cathode delivers an initial discharge capacity of 909.4 mAh g^{-1} and remains at 656.6 mAh g^{-1} after 500 cycles with a capacity retention of 72% and average columbic efficiency of 99.8%. Such extraordinary cycling performance of the Co@NC/S cathode outperforms those of NC/S, Co/S, and physically mixed Co/NC/S cathodes (Figure S25), revealing the important role of the Mott−Schottky interfacial effect rather than the synergistic effect between Co and NC in Li−S chemistry. Note that the capacity contribution from the Co@NC heterostructure is negligible (Figure S26). Under a much higher rate of 4 *C*, the Li−S battery with a Co@NC electrocatalyst also achieves unparalleled cycling stability with a capacity retention of 93.0% after 800 cycles (Figure 4d and Figure S27), which is prominent in comparison to other state-of-the-art Li−S studies on catalytic cathode hosts as summarized in Table S1.

To analyze the structural integrity of cathodes and anodes, we also disassembled from the Li−S cells after 100 cycles at 1 *C*. From the post-mortem SEM image in Figure 4e, one can discern seriously passivated NC/S cathode with large agglomerations on the rough surface. Conversely, the cycled Co@NC/S cathode almost retains its original morphology and exhibits a relatively smooth surface that only contains uniform solid precipitates with no obvious large aggregations.[39] As for the Li metal anode paired with the NC cathode (Figure 4f), it unveils a looser and rougher surface and many conspicuous cracks. In comparison, the cycled Li anode from the Co@NC/S cell still maintains a roughly compact surface with few pores/voids. Furthermore, the Li anode and separator from the Co@NC cell exhibit a much lighter color than that from the NC/S cell (Figure S28), further revealing that Co@NC helps to alleviate LiPSs shuttling and stabilize the S cathode and Li anode, which also helps to maintain low charge-transfer resistance during cycling, as shown in the Nyquist plots (Figure S29).

To demonstrate the utilization of Mott−Schottky heterostructure in practical high-energy-density Li−S batteries, we also prepared Co@NC/S cathode with ultrahigh loading of 10.73 mg cm^{-2} and cycled the cathode under starved electrolyte (E/S = 5.9 μL mg^{-1}). As displayed in Figure 4g, the cathode displays an initial capacity of 6.74 mAh cm^{-2} at 0.2 *C*, which increases to 8.17 mAh cm^{-2} after 17 cycles due to the activation process of the sulfur cathode as often observed in the literature.[40,41] A reversible capacity of 6.21 mAh cm^{-2} after 120 cycles remains with overall capacity retention as high as 92.1%, which compares favorably with recently reported sulfur cathodes with raised loading (>5 mg cm^{-2}), as displayed in Figure 4h and Table S2. More crucially, at a current rate of 0.05 C, Co@NC/S cathode releases a high areal capacity of 12.87 mAh cm^{-2} (Figure S32). Accordingly, the gravimetric energy density is calculated to be 307.8 Wh kg^{-1} at a system level (see details in Table S3), which outperforms most of the previously reported Li−S batteries (usually <200 Wh kg^{-1}) (see details in Table S4).

High-temperature tolerance is another priority on the way to commercial Li−S batteries.[42] At 55 °C (Figure S34), the Co@NC/S cathode exhibits a maximum areal capacity of 4.05 mAh cm^{-2} and maintains 80.3% after 60 cycles under a sulfur loading of 4.29 mg cm^{-2} at 0.2 *C*. These capacities and cyclabilities are much better than those of a NC/S cathode and highly competitive among the recently reported works on high-temperature Li−S batteries (see details in Table S5), indicating that the Mott−Schottky heterojunction could be a new type of catalytic cathode host for advanced high-energy-density Li−S batteries.

In conclusion, we employed the Co@NC Mott−Schottky heterostructure as a cathode host to catalyze conversion chemistry in Li−S batteries. The strongly coupled Co nanoparticles and porous N-doped C matrix induces self-driven charge redistribution and a built-in electronic field at the interface, which helps to propel Li^+/e^- transport rates, chemisorb polysulfide species, reduce energy barrier for polysulfide reduction, and Li_2S oxidation in the discharge/charge processes. Benefiting from this Mott−Schottky catalytic effect, the Li−S batteries built with Co@NC catalysts exhibit impressive capacity retention (92.1%) and gravimetric energy density (307.8 Wh kg^{-1}) under ultrahigh sulfur loading (10.73 mg cm^{-2}) and lean electrolyte (5.9 μL mg^{-1}) conditions. The present work deepens the understanding of the Mott−Schottky catalytic mechanism for high-efficiency Li−S conversion chemistry and broadens the horizons of electrocatalyst design for other multielectron energy storage and conversion systems.

■ ASSOCIATED CONTENT

Supporting Information

The Supporting Information is available free of charge at https://pubs.acs.org/doi/10.1021/acs.nanolett.1c02161.

Experimental details, SEM/TEM images, XRD patterns, pore size distribution, Raman spectra, adsorption−desorption isotherms, TGA curves, XPS survey spectra, UPS spectra, digital images, CV curves, EIS spectra, Tafel plots, Nyquist plots, galvanostatic charge−discharge profiles, rate and cycling performances, comparison charts, and design parameters (PDF)

■ AUTHOR INFORMATION

Corresponding Author

Yongming Sun − *Wuhan National Laboratory for Optoelectronics, Huazhong University of Science and Technology, Wuhan 430074, China;* orcid.org/0000-0001-8528-525X; Email: yongmingsun@hust.edu.cn

Authors

Yuanjian Li − *Wuhan National Laboratory for Optoelectronics, Huazhong University of Science and Technology, Wuhan 430074, China*

Wenyu Wang − *Wuhan National Laboratory for Optoelectronics, Huazhong University of Science and Technology, Wuhan 430074, China*

Bao Zhang − *School of Optical and Electronic information, Huazhong University of Science and Technology, Wuhan 430074, China;* orcid.org/0000-0003-3236-221X

https://doi.org/10.1021/acs.nanolett.1c02161
Nano Lett. XXXX, XXX, XXX−XXX

Lin Fu − *Wuhan National Laboratory for Optoelectronics, Huazhong University of Science and Technology, Wuhan 430074, China;* orcid.org/0000-0001-6834-2881
Mintao Wan − *Wuhan National Laboratory for Optoelectronics, Huazhong University of Science and Technology, Wuhan 430074, China*
Guocheng Li − *Wuhan National Laboratory for Optoelectronics, Huazhong University of Science and Technology, Wuhan 430074, China*
Zhao Cai − *Wuhan National Laboratory for Optoelectronics, Huazhong University of Science and Technology, Wuhan 430074, China;* orcid.org/0000-0001-7110-9300
Shuibin Tu − *Wuhan National Laboratory for Optoelectronics, Huazhong University of Science and Technology, Wuhan 430074, China*
Xiangrui Duan − *Wuhan National Laboratory for Optoelectronics, Huazhong University of Science and Technology, Wuhan 430074, China*
Zhi Wei Seh − *Institute of Materials Research and Engineering, Agency for Science, Technology and Research (A*STAR), 138634, Singapore;* orcid.org/0000-0003-0953-567X
Jianjun Jiang − *School of Optical and Electronic information, Huazhong University of Science and Technology, Wuhan 430074, China;* orcid.org/0000-0001-9178-8988

Complete contact information is available at: https://pubs.acs.org/10.1021/acs.nanolett.1c02161

Author Contributions

[⊥]Y.L., W.W., and B.Z. contributed equally to this work.

Notes

The authors declare no competing financial interest.

■ ACKNOWLEDGMENTS

Y.S. acknowledges the financial support by the National Natural Science Foundation of China (52002136 and 51802105) and the Innovation Fund of Wuhan National Laboratory for Optoelectronics of Huazhong University of Science and Technology. B.Z. acknowledges the support by the China Postdoctoral Science Foundation (2020M682400). Z.C. thanks the China Postdoctoral Science Foundation (2018M640694 and 2020T130223). Z.W.S. acknowledges the support of the Singapore National Research Foundation (NRF-NRFF2017-04). The authors would like to thank the Analytical and Testing Center of Huazhong University of Science and Technology as well as the Center for Nanoscale Characterization & Devices of Wuhan National Laboratory for Optoelectronics for providing the facilities to conduct the characterization.

■ REFERENCES

(1) Seh, Z. W.; Sun, Y.; Zhang, Q.; Cui, Y. Designing high-energy lithium-sulfur batteries. *Chem. Soc. Rev.* **2016**, *45*, 5605−5634.
(2) Bruce, P. G.; Freunberger, S. A.; Hardwick, L. J.; Tarascon, J. M. Li-O_2 and Li-S batteries with high energy storage. *Nat. Mater.* **2012**, *11*, 19−29.
(3) Hu, A.; Zhou, M.; Lei, T.; Hu, Y.; Du, X.; Gong, C.; Shu, C.; Long, J.; Zhu, J.; Chen, W.; et al. Optimizing redox reactions in aprotic lithium-sulfur batteries. *Adv. Energy Mater.* **2020**, *10*, 2002180.
(4) Zhao, C.; Xu, G. L.; Yu, Z.; Zhang, L.; Hwang, I.; Mo, Y. X.; Ren, Y.; Cheng, L.; Sun, C. J.; Ren, Y.; Zuo, X.; Li, J. T.; Sun, S. G.; Amine, K.; Zhao, T. A high-energy and long-cycling lithium-sulfur pouch cell via a macroporous catalytic cathode with double-end binding sites. *Nat. Nanotechnol.* **2021**, *16*, 166−173.
(5) Tu, S.; Chen, X.; Zhao, X.; Cheng, M.; Xiong, P.; He, Y.; Zhang, Q.; Xu, Y. A polysulfide-immobilizing polymer retards the shuttling of polysulfide intermediates in lithium-sulfur batteries. *Adv. Mater.* **2018**, *30*, 1804581.
(6) Li, Y.; Wang, W.; Liu, X.; Mao, E.; Wang, M.; Li, G.; Fu, L.; Li, Z.; Eng, A. Y. S.; Seh, Z. W.; Sun, Y. Engineering stable electrode-separator interfaces with ultrathin conductive polymer layer for high-energy-density Li-S batteries. *Energy Storage Mater.* **2019**, *23*, 261−268.
(7) Peng, L.; Wei, Z.; Wan, C.; Li, J.; Chen, Z.; Zhu, D.; Baumann, D.; Liu, H.; Allen, C. S.; Xu, X.; Kirkland, A. I.; Shakir, I.; Almutairi, Z.; Tolbert, S.; Dunn, B.; Huang, Y.; Sautet, P.; Duan, X. A fundamental look at electrocatalytic sulfur reduction reaction. *Nat. Catal.* **2020**, *3*, 762−770.
(8) Wang, R.; Luo, C.; Wang, T.; Zhou, G.; Deng, Y.; He, Y.; Zhang, Q.; Kang, F.; Lv, W.; Yang, Q. H. Bidirectional catalysts for liquid-solid redox conversion in lithium-sulfur batteries. *Adv. Mater.* **2020**, *32*, 2000315.
(9) Zhou, G.; Tian, H.; Jin, Y.; Tao, X.; Liu, B.; Zhang, R.; Seh, Z. W.; Zhuo, D.; Liu, Y.; Sun, J.; Zhao, J.; Zu, C.; Wu, D. S.; Zhang, Q.; Cui, Y. Catalytic oxidation of Li_2S on the surface of metal sulfides for Li−S batteries. *Proc. Natl. Acad. Sci. U. S. A.* **2017**, *114*, 840−845.
(10) Zhou, G.; Zhao, S.; Wang, T.; Yang, S. Z.; Johannessen, B.; Chen, H.; Liu, C.; Ye, Y.; Wu, Y.; Peng, Y.; Liu, C.; Jiang, S. P.; Zhang, Q.; Cui, Y. Theoretical calculation guided design of single-atom catalysts toward fast kinetic and long-life Li-S batteries. *Nano Lett.* **2020**, *20*, 1252−1261.
(11) Li, Y.; Wang, C.; Wang, W.; Eng, A. Y. S.; Wan, M.; Fu, L.; Mao, E.; Li, G.; Tang, J.; Seh, Z. W.; Sun, Y. Enhanced chemical immobilization and catalytic conversion of polysulfide intermediates using metallic Mo nanoclusters for high-performance Li-S batteries. *ACS Nano* **2020**, *14*, 1148−1157.
(12) Li, Y.; Wu, J.; Zhang, B.; Wang, W.; Zhang, G.; Seh, Z. W.; Zhang, N.; Sun, J.; Huang, L.; Jiang, J.; Zhou, J.; Sun, Y. Fast conversion and controlled deposition of lithium (poly)sulfides in lithium-sulfur batteries using high-loading cobalt single atoms. *Energy Storage Mater.* **2020**, *30*, 250−259.
(13) Xue, W.; Shi, Z.; Suo, L.; Wang, C.; Wang, Z.; Wang, H.; So, K. P.; Maurano, A.; Yu, D.; Chen, Y.; Qie, L.; Zhu, Z.; Xu, G.; Kong, J.; Li, J. Intercalation-conversion hybrid cathodes enabling Li-S full-cell architectures with jointly superior gravimetric and volumetric energy densities. *Nat. Energy* **2019**, *4*, 374−382.
(14) Li, G.; Lei, W.; Luo, D.; Deng, Y.; Deng, Z.; Wang, D.; Yu, A.; Chen, Z. Stringed "tube on cube" nanohybrids as compact cathode matrix for high-loading and lean-electrolyte lithium-sulfur batteries. *Energy Environ. Sci.* **2018**, *11*, 2372−2381.
(15) Zhou, J.; Liu, X.; Zhu, L.; Zhou, J.; Guan, Y.; Chen, L.; Niu, S.; Cai, J.; Sun, D.; Zhu, Y.; Du, J.; Wang, G.; Qian, Y. Deciphering the modulation essence of p bands in Co-based compounds on Li-S chemistry. *Joule* **2018**, *2*, 2681−2693.
(16) Shen, Z.; Zhang, Z.; Li, M.; Yuan, Y.; Zhao, Y.; Zhang, S.; Zhong, C.; Zhu, J.; Lu, J.; Zhang, H. Rational design of a $Ni_3N_{0.85}$ electrocatalyst to accelerate polysulfide conversion in lithium-sulfur batteries. *ACS Nano* **2020**, *14*, 6673−6682.
(17) Yuan, H.; Peng, H.-J.; Li, B.-Q.; Xie, J.; Kong, L.; Zhao, M.; Chen, X.; Huang, J.-Q.; Zhang, Q. Conductive and catalytic triple-phase interfaces enabling uniform nucleation in high-rate lithium-sulfur batteries. *Adv. Energy Mater.* **2018**, *8*, 1802768.
(18) Liu, Y. X.; Wang, H. H.; Zhao, T. J.; Zhang, B.; Su, H.; Xue, Z. H.; Li, X. H.; Chen, J. S. Schottky barrier induced coupled interface of electron-rich N-doped carbon and electron-deficient Cu: in-built Lewis acid-base pairs for highly efficient CO_2 fixation. *J. Am. Chem. Soc.* **2019**, *141*, 38−41.
(19) Zhong, Y.; Yin, L.; He, P.; Liu, W.; Wu, Z.; Wang, H. Surface chemistry in cobalt phosphide-stabilized lithium-sulfur batteries. *J. Am. Chem. Soc.* **2018**, *140*, 1455−1459.

(20) Wang, Y.; Zhang, R.; Sun, Z.; Wu, H.; Lu, S.; Wang, J.; Yu, W.; Liu, J.; Gao, G.; Ding, S. Spontaneously formed Mott-Schottky electrocatalyst for lithium-sulfur batteries. *Adv. Mater. Interfaces* **2020**, *7*, 1902092.
(21) Cheng, Z.; Chen, Y.; Yang, Y.; Zhang, L.; Pan, H.; Fan, X.; Xiang, S.; Zhang, Z. Metallic MoS_2 nanoflowers decorated graphene nanosheet catalytically boosts the volumetric capacity and cycle life of lithium-sulfur batteries. *Adv. Energy Mater.* **2021**, *11*, 2003718.
(22) Liu, J.; Li, W.; Duan, L.; Li, X.; Ji, L.; Geng, Z.; Huang, K.; Lu, L.; Zhou, L.; Liu, Z.; Chen, W.; Liu, L.; Feng, S.; Zhang, Y. A graphene-like oxygenated carbon nitride material for improved cycle-life lithium/sulfur batteries. *Nano Lett.* **2015**, *15*, 5137−5142.
(23) Zhang, C.; Du, R.; Biendicho, J. J.; Yi, M.; Xiao, K.; Yang, D.; Zhang, T.; Wang, X.; Arbiol, J.; Llorca, J.; Zhou, Y.; Morante, J. R.; Cabot, A. Tubular CoFeP@CN as a Mott-Schottky catalyst with multiple adsorption sites for robust lithium-sulfur batteries. *Adv. Energy Mater.* **2021**, *11*, 2100432.
(24) Zhang, L.; Chen, X.; Wan, F.; Niu, Z.; Wang, Y.; Zhang, Q.; Chen, J. Enhanced electrochemical kinetics and polysulfide traps of indium nitride for highly stable lithium-sulfur batteries. *ACS Nano* **2018**, *12*, 9578−9586.
(25) Li, C.; Liu, Y.; Zhuo, Z.; Ju, H.; Li, D.; Guo, Y.; Wu, X.; Li, H.; Zhai, T. Local charge distribution engineered by schottky heterojunctions toward urea electrolysis. *Adv. Energy Mater.* **2018**, *8*, 1801775.
(26) Sun, Z.; Wang, Y.; Zhang, L.; Wu, H.; Jin, Y.; Li, Y.; Shi, Y.; Zhu, T.; Mao, H.; Liu, J.; Xiao, C.; Ding, S. Simultaneously realizing rapid electron transfer and mass transport in jellyfish-like Mott-Schottky nanoreactors for oxygen reduction reaction. *Adv. Funct. Mater.* **2020**, *30*, 1910482.
(27) Dong, Y.; Liu, Y.; Hu, Y.; Ma, K.; Jiang, H.; Li, C. Boosting reaction kinetics and reversibility in Mott-Schottky VS_2/MoS_2 heterojunctions for enhanced lithium storage. *Sci. Bull.* **2020**, *65*, 1470−1478.
(28) Li, X.; Pan, Y.; Yi, H.; Hu, J.; Yang, D.; Lv, F.; Li, W.; Zhou, J.; Wu, X.; Lei, A.; Zhang, L. Mott-Schottky effect leads to alkyne semihydrogenation over Pd-nanocube@N-doped carbon. *ACS Catal.* **2019**, *9*, 4632−4641.
(29) Li, Y.-J.; Fan, J.-M.; Zheng, M.-S.; Dong, Q.-F. A novel synergistic composite with multi-functional effects for high-performance Li-S batteries. *Energy Environ. Sci.* **2016**, *9*, 1998−2004.
(30) Ma, L.; Lin, H.; Zhang, W.; Zhao, P.; Zhu, G.; Hu, Y.; Chen, R.; Tie, Z.; Liu, J.; Jin, Z. Nitrogen-doped carbon nanotube forests planted on cobalt nanoflowers as polysulfide mediator for ultralow self-discharge and high areal-capacity lithium-sulfur batteries. *Nano Lett.* **2018**, *18*, 7949−7954.
(31) Wang, R.; Yang, J.; Chen, X.; Zhao, Y.; Zhao, W.; Qian, G.; Li, S.; Xiao, Y.; Chen, H.; Ye, Y.; Zhou, G.; Pan, F. Highly dispersed cobalt clusters in nitrogen-doped porous carbon enable multiple effects for high-performance Li-S battery. *Adv. Energy Mater.* **2020**, *10*, 1903550.
(32) Wu, Q.; Zhou, X.; Xu, J.; Cao, F.; Li, C. Adenine derivative host with interlaced 2D structure and dual lithiophilic-sulfiphilic sites to enable high-loading Li-S batteries. *ACS Nano* **2019**, *13*, 9520−9532.
(33) Lin, H.; Zhang, S.; Zhang, T.; Cao, S.; Ye, H.; Yao, Q.; Zheng, G. W.; Lee, J. Y. A Cathode-integrated sulfur-deficient Co_9S_8 catalytic interlayer for the reutilization of "lost" polysulfides in lithium-sulfur batteries. *ACS Nano* **2019**, *13*, 7073−7082.
(34) Cao, Y.; Wu, H.; Li, G.; Liu, C.; Cao, L.; Zhang, Y.; Bao, W.; Wang, H.; Yao, Y.; Liu, S.; Pan, F.; Jiang, Z.; Sun, J. Ion selective covalent organic framework enabling enhanced electrochemical performance of lithium-sulfur batteries. *Nano Lett.* **2021**, *21*, 2997−3006.
(35) Yu, M.; Zhou, S.; Wang, Z.; Wang, Y.; Zhang, N.; Wang, S.; Zhao, J.; Qiu, J. Accelerating polysulfide redox conversion on bifunctional electrocatalytic electrode for stable Li-S batteries. *Energy Storage Mater.* **2019**, *20*, 98−107.
(36) Luo, C.; Liang, X.; Sun, Y.; Lv, W.; Sun, Y.; Lu, Z.; Hua, W.; Yang, H.; Wang, R.; Yan, C.; Li, J.; Wan, Y.; Yang, Q.-H. An organic nickel salt-based electrolyte additive boosts homogeneous catalysis for lithium-sulfur batteries. *Energy Storage Mater.* **2020**, *33*, 290−297.
(37) Wang, T. S.; Liu, X.; Zhao, X.; He, P.; Nan, C. W.; Fan, L. Z. Regulating uniform Li plating/stripping via dual-conductive metal-organic frameworks for high-rate lithium metal batteries. *Adv. Funct. Mater.* **2020**, *30*, 2000786.
(38) Du, Z.; Chen, X.; Hu, W.; Chuang, C.; Xie, S.; Hu, A.; Yan, W.; Kong, X.; Wu, X.; Ji, H.; Wan, L. J. Cobalt in nitrogen-doped graphene as single-atom catalyst for high-sulfur content lithium-sulfur batteries. *J. Am. Chem. Soc.* **2019**, *141*, 3977−3985.
(39) Chen, Y.; Li, Z.; Li, X.; Zeng, D.; Xu, G.; Zhang, Y.; Sun, Y.; Ke, H.; Cheng, H. Harvesting polysulfides by sealing the sulfur electrode in a composite ion-selective net. *J. Power Sources* **2017**, *368*, 38−45.
(40) Li, Z.; Zhang, J.; Lu, Y.; Lou, X. W. A pyrolyzed polyacrylonitrile/selenium disulfide composite cathode with remarkable lithium and sodium storage performances. *Sci. Adv.* **2018**, *4*, No. eaat1687.
(41) Hu, A.; Chen, W.; Du, X.; Hu, Y.; Lei, T.; Wang, H.; Xue, L.; Li, Y.; Sun, H.; Yan, Y.; et al. An artificial hybrid interphase for an ultrahigh-rate and partical lithium metal anode. *Energy Environ. Sci.* **2021**, *14*, 4115−4124.
(42) Deng, D. R.; Xue, F.; Bai, C. D.; Lei, J.; Yuan, R.; Zheng, M. S.; Dong, Q. F. Enhanced adsorptions to polysulfides on graphene-supported BN nanosheets with excellent Li-S battery performance in a wide temperature range. *ACS Nano* **2018**, *12*, 11120−11129.

https://doi.org/10.1021/acs.nanolett.1c02161
Nano Lett. XXXX, XXX, XXX−XXX